An insight into the influence of morphological and compositional heterogeneity of an individual intermetallic particle on aluminium alloy corrosion initiation

A. Davoodi*, J. Pan, C. Leygraf, R. Parvizi and S. Norgren

In this work, a multi-analytical *in situ* and *ex situ* approach was used to provide information needed to identify the role of an individual heterogeneous intermetallic particle (IMP) in localized corrosion initiation of aluminium alloys. The heterogeneity of the IMP was studied by combining atomic force microscopy (AFM), scanning electron microscopy and energy dispersive spectroscopy (SEM–EDS) and scanning electrochemical microscopy (SECM). A complex Al–Mn–Fe–Si IMP phase with different chemical composition in its inner and outer parts was characterized by SEM–EDS analysis. AFM results uniquely revealed a brain-like feature of an IMP with 20 nm height variations. Submicron sized galvanic cell induced by morphological and compositional heterogeneity resulted in a localized corrosion attack inside the individual IMP. Various collected current levels measured by SECM were associated to the morphological and compositional heterogeneity of IMPs.

1 Introduction

Aluminium alloys are of interest for various applications particularly due to their good corrosion resistance and recyclability potential [1]. During the manufacturing processes, elemental additives may create various kinds of insoluble intermetallic particles (IMPs) in the alloys and influence the final product properties [2–7]. The second phases are either cathodic or anodic compared to the aluminium matrix resulting in galvanic cell formation, due to the potential difference between these constituent phases, which leads to the local degradation of aluminium alloys in chloride-containing media [8–10]. Literature reports on pitting corrosion of aluminium alloys have pointed out the necessitation to further explore the microstructure complexities and influence of the second phases such as formation of pits

on IMPs [8, 10–12]. Characterization of IMPs by various techniques has been the target of scientific studies for decades [1, 9, 11, 13–19]. Three aspects are vital during characterization of IMPs: lateral resolution, analytical capability and *in situ* performance [17, 18, 20, 21]. However, none of the used techniques can individually provide all the information needed for characterizing the role of IMPs. In this work, a combination of *in situ* and *ex situ* atomic force microscopy (AFM), scanning electron microscopy and energy dispersive spectroscopy (SEM–EDS) and scanning electrochemical microscopy (SECM) techniques was employed to assess the morphological, compositional and chemical heterogeneity of an individual IMP in corrosion initiation of a wrought aluminium alloy (AA3003, an Al–Mn alloy).

2 Materials and methods

The chemical composition of the alloy (in wt%) was 1.1% Mn, 0.50% Fe, 0.13% Si, 0.11% Cu and Al as balance [8, 22, 23]. Philips XL30S FEG-SEM instrument was used for microstructure characterization and elemental analysis of the IMPs. An extraction method was applied on small particles. In this method, Al alloy samples were dissolved at 117 °C in an argon atmosphere in distilled butanol and continuously dried in air. After dissolution process, butanol and aluminium oxide were filtered through a teflon filter. The undissolved particles on the teflon filter were analyzed by the use of X-ray diffractometer, SEM and microprobe analysis. The AFM instrument used was a Resolver from Quesant (Ambios Technology), USA, in contact mode, *ex situ* in air and *in situ* in solution, was used to get topography

A. Davoodi
Department of Materials Science Engineering, Sabzevar Tarbiat Moallem University, Sabzevar 391 (Iran)
E-mail: adavoodi@kth.se

J. Pan, C. Leygraf
Division of Surface and Corrosion Science, KTH Royal Institute of Technology, Drottning Kristinas väg. 51, SE-10044 Stockholm (Sweden)

R. Parvizi
Materials and Metallurgical Engineering Department, Ferdowsi University of Mashhad, Mashhad (Iran)

S. Norgren
Sapa Technology, SE-612 81 Finspång (Sweden)

images. High resolution SECM from Windsor Scientific ltd *iprobe* instrument equipped with a bipotentiostat (four-electrode configuration) was used in 20 mM diluted NaCl solution to map the electrochemical activity. A calibrated SECM ultra-microelectrode (UME), a platinum tip with radius of about 500 nm, was used to collect the local currents on aluminium surface. AFM and SECM were operated in contact and sample generation tip-collection (sample generation-tip collection by using KI as redox mediator) modes, respectively. In order to report the local currents recorded on every individual surface constituent, an image analysis was performed for current fraction calculation on individual surface constituents [8, 22].

3 Results and discussion

Figure 1a shows the backscatter electron (BSE)-SEM micrograph of an individual IMP. It is found that the dark matrix mainly
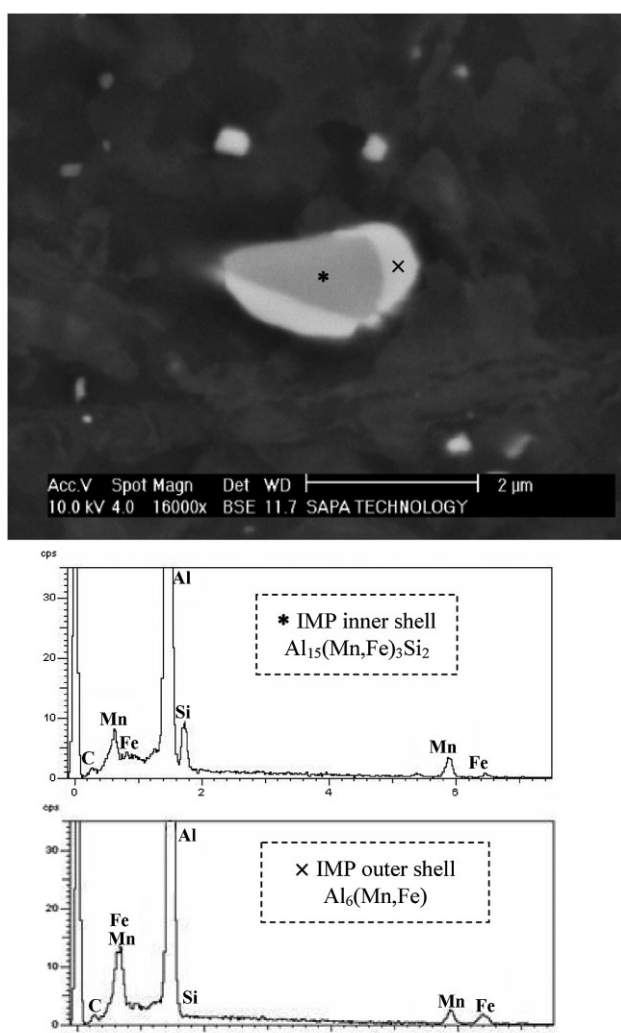

Figure 1. BSE-SEM micrograph showing the complexity of an individual heterogeneous IMP with different chemical compositions in its inner and outer parts and corresponding EDS results. Some dispersoids also exist

consists of the light Al element. Several small dispersoids and a large complex IMP with different chemical composition in its inner and outer parts were observed and confirmed by EDS results in Fig. 1b. Generally, in AA3003 alloy, there are two distinct types of eutectically formed IMPs (with divergent size factors) [ref]: the α-Al(Mn,Fe)Si phase, typically $Al_{15}(Mn,Fe)_3Si_2$, and the Al(Mn,Fe) phase, typically $Al_6(Mn,Fe)$, where the latter appears brighter (due to higher molar weight) in the BSE-SEM images. Within the measuring accuracy the EDS results depict that for the specific IMP in Fig. 1a, the outer shell of the two-component IMP has the same chemical composition as $Al_6(Mn,Fe)$ phase, which is very close to fine round dispersoids containing heavier elements. In contrast, the darker inner constituent suggests the chemical composition of $Al_{15}(Mn,Fe)_3Si_2$. The chemical heterogeneity of an IMP may be attributed to several processes such as a coarsening phenomenon, atomic scale partitioning, solvent migration and diffusion of atoms from the matrix to different constituent phases [2–5, 14, 17, 23]. The variation in composition of the inner and outer parts of the IMP depends on the Fe and Si contents and the difference in Mn/Fe ratio. Apparently, similar to dispersoids, the outer layer is nucleated and formed during the secondary hot rolling and subsequent heat treatment stages where the inner part, $Al_{15}(Mn,Fe)_3Si_2$ phase, acts as a nuclei in a limited diffusion distance [2–5, 17, 23].

Surface conditions may change during sample transfer for post-exposure SEM examination and it does not give information on the third dimension perpendicular to the surface. To overcome these limitations, high lateral and spatial resolution AFM and SECM were used to visualize the corrosion attack at and around the selected IMP. Figure 2a demonstrates the morphological details of an individual IMP obtained by *ex situ* AFM. The image shows the heterogeneous morphology of the IMP uniquely observed by high resolution AFM. A dispersoid also exists in the left side of the larger IMP in Fig. 2a. Clearly the IMP exhibits a heterogeneous morphology while the small size dispersoid demonstrates almost a uniform homogenous appearance. With surface topography analysis, an average roughness (R_p) value of less than 20 nm was observed. During the solidification process, such IMPs are formed multi-directionally and create a particular brain-like feature as shown in Fig. 2a. Previous result obtained by SEM on a corroded Al–Mn alloy also revealed such a heterogeneity, as shown in Fig. 2b [10]. Interestingly, similar features could be seen in both AFM and SEM images where pits initiated not only in the adjacent matrix and the IMP/matrix interface, but also inside the IMP itself [10, 11, 14].

Figure 3 shows the *in situ* SECM result and the corresponding current profile across three individual active sites during current collection at a 200 mV anodic overpotential (with respect to the corrosion potential). The current levels can be individually related to the microstructure heterogeneity [22]. To make a dimensionless comparison, local current densities were estimated based on calculated surface areas measured by previous SEM and AFM images. As shown in the SECM image and the current profile, by applying a 200 mV anodic overpotential, three current levels could be detected. The lowest current value is attributed to the IMP cathodic sites with about 29% fraction of the scanned area and a current density of 180 μA/cm^2. All current
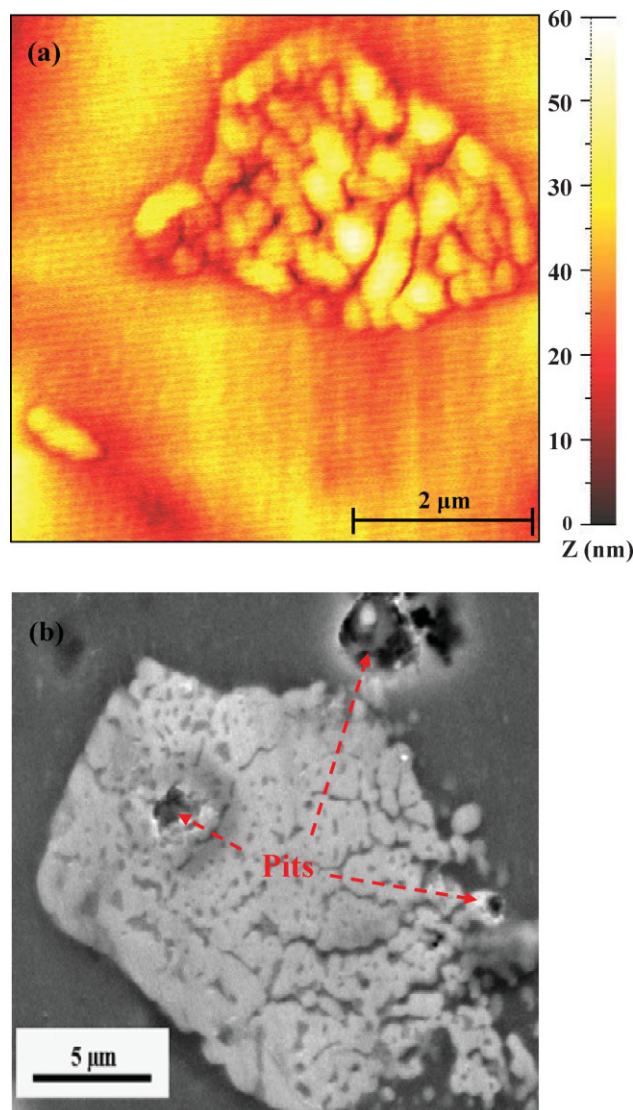
Figure 2. (a) *Ex situ* AFM image of an individual IMP and a dispersoid on polished AA3003 Al alloy showing the heterogeneity of an individual IMP with the surface roughness of less than 20 nm and (b) SEM image of an attacked Al–Mn–Fe IMP in naturally aerated 0.1 M NaCl solution. The morphology details of an individual IMP and pitting sites is observed inside the IMP itself, at the IMP edge and in the adjacent matrix [10] reprinted with permission

Figure 3. (a) High resolution *in situ* SECM image of AA3003 alloy in 20 mM NaCl solution and (b) a line profile across three individual active sites indicating heterogeneous currents origination. Currents were captured on the sample instantly at 200 mV anodic overpotential, collected locally by Pt ultra-microelectrode (adjusted at 700 mV *vs.* Ag/AgCl). Highest current peaks correspond to the trench formed around IMPs. SECM tip radius was 500 nm, scan area $15 \times 15\,\mu m^2$ and scan rate 1 Hz

density values were calculated based on the absolute current values measured by SECM tip divided by the corresponding effective surface area of each individual surface constituent, including the matrix itself. The higher current level is from the matrix area with about 55% fraction of the scanned area and corresponds to a current density of $110\,\mu A/cm^2$. The highest current value is generated by trenches formed either around or inside an individual IMP with about 16% fraction of the scanned area and corresponds to a current density of $440\,\mu A/cm^2$. Eventually, the applied anodic overpotential leads to trench (or other localized active sites) formation and significant increase in dissolution current density (measured indirectly from the redox mediator). By comparing the t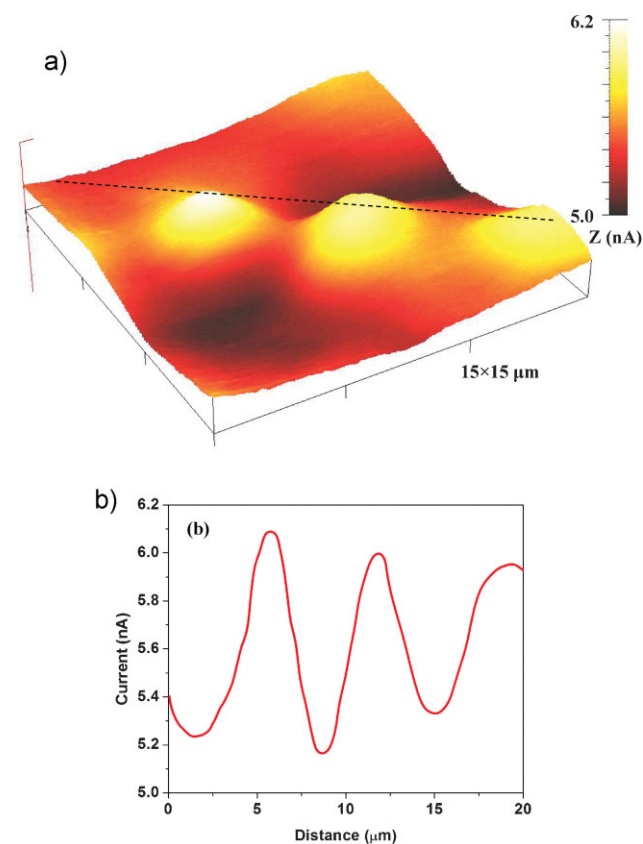hree calculated current densities, it can be concluded that the highest generated current density is attributed to the localized corrosion sites, such as trenches at the IMP/matrix interface or at the inner/outer shell interface of an individual IMP [22]. It is noticeable that, despite the higher local current level of the matrix, the cathodic sites on the IMP owe higher current density compared to the surrounding matrix. This indicates that phase fraction calculation (compare with comment above, one never introduced this concept before) can be employed as a method for precisely determination of generated/collected current densities. Although the results obtained from SECM demonstrate that the cathodic reduction reaction occurred at the sites adjacent to inclusions, the heterogeneous microstructure of the studied IMPs can supply other active sites for cathodic or anodic reactions.

An *in situ* AFM image in Fig. 4 represents the dissolution morphology of an individual Al–Mn–Fe–Si IMP on the AA3003 sample surface due to induction of an internal/external microgalvanic couple (with matrix as anode) in naturally aerated 3.5% NaCl. A ring-like porous corrosion product with around 400 nm height in Z-direction was observed around the pit, at the location of an IMP. This can be related to the accumulation of the
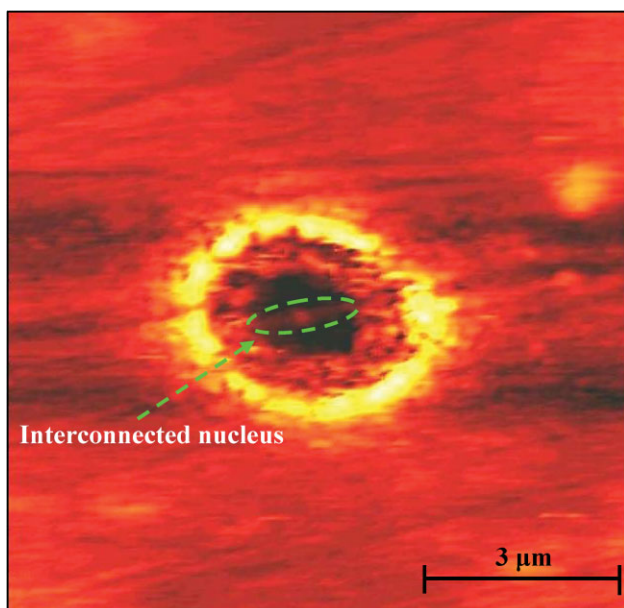
Figure 4. Topography of a dissolved Al–Mn–Fe IMP on AA3003 alloy in naturally aerated 3.5% NaCl solution obtained by *in situ* AFM

corrosion products resulting from IMP dissolution. It confirms the detachment mechanisms previously proposed by other authors [9, 11]. Intriguingly, by precisely investigating the pit morphology in Fig. 4, an interconnected nucleus is also observed in the middle of the pit which may be the origin of the brain-like IMP formation that still remains after deterioration. In summary, considering the results in Figs. 1–4, the observed dissolution of the IMP is the result of microgalvanic corrosion caused by the chemically and morphologically different constituents [2, 8, 10, 11, 15, 18].

4 Conclusions

Morphological and chemical heterogeneity of a particular IMP in AA3003 aluminium alloy has been studied by combination of AFM, SEM–EDS and SECM. It was shown that the chemical and morphological heterogeneity of the IMP structure affects the alloy electrochemical corrosion attack sites on the IMP itself, at the particle edge and in the adjacent matrix. Moreover, using sophisticated nanosize SECM makes it possible to collect the electrochemical current close proximity distance from the aluminium alloy surface associated to the morphological and compositional heterogeneity of IMPs.

5 References

[1] C. S. Paglia, R. G. Buchheit, *Scr. Mater.* **2008**, *58*, 383.
[2] M. Warmuzek, W. Ratuszek, G. Sek-Sas, *Mater. Charact.* **2005**, *54*, 31.
[3] W. C. Liu, B. Radhakrishnan, *Mater. Lett.* **2010**, *64*, 1829.
[4] N. A. Belov, D. G. Eskin, A. A. Aksenov, in: *Multicomponent Phase Diagrams*, Elsevier, Oxford **2005**, pp. 1–46.
[5] D. T. L. Alexander, A. L. Greer, *Philos. Mag.* **2004**, *84*, 3071.
[6] E. Ghali, *Corrosion Resistance of Aluminum and Magnesium Alloys*, John Wiley & Sons, Inc, Hoboken, New Jersey **2010**.
[7] C. Vargel, M. Jacques, M. P. Schmidt, *Corrosion of Aluminium*, 1 Edn., Elsevier Ltd, Amsterdam **2004**.
[8] A. Davoodi, J. Pan, C. Leygraf, S. Norgren, *J. Electrochem. Soc.* **2008**, *155*, C211.
[9] G. O. Ilevbare, O. Schneider, R. G. Kelly, J. R. Scully, *J. Electrochem. Soc.* **2004**, *151*, B453.
[10] S. Ghosh, in: *Metallurgy and Materials*, University of Birmingham, Birmingsham **2008**, p. 434.
[11] A. Boag, A. E. Hughes, N. C. Wilson, A. Torpy, C. M. MacRae, A. M. Glenn, T. H. Muster, *Corros. Sci.* **2009**, *51*, 1565.
[12] M. K. Cavanaugh, N. Birbilis, R. G. Buchheit, F. Bovard, *Scr. Mater.* **2007**, *56*, 995.
[13] Y. Liu, X. Zhou, G. E. Thompson, T. Hashimoto, G. M. Scamans, A. Afseth, *Acta Mater.* **2007**, *55*, 353.
[14] J. Wloka, S. Virtanen, *Acta Mater.* **2007**, *55*, 6666.
[15] N. Birbilis, R. G. Buchheit, *J. Electrochem. Soc.* **2005**, *152*, B140.
[16] V. Guillaumin, P. Schmutz, G. S. Frankel, *J. Electrochem. Soc.* **2001**, *148*, B163.
[17] P. J. E. Forsyth, *Mater. Lett.* **1992**, *13*, 184.
[18] T. Hashimoto, X. Zhou, C. Luo, K. Kawano, G. E. Thompson, A. E. Hughes, P. Skeldon, P. J. Withers, T. J. Marrow, A. H. Sherry, *Scr. Mater.* **2010**, *63*, 835.
[19] T. Rayment, A. J. Davenport, A. J. Dent, J.-P. Tinnes, R. J. K. Wiltshire, C. Martin, G. Clark, P. Quinn, J. F. W. Mosselmans, *Electrochem. Commun.* **2008**, *10*, 855.
[20] Y. González-García, S. J. García, A. E. Hughes, J. M. C. Mol, *Electrochem. Commun.* **2011**, *13*, 1094.
[21] Y. González-García, J. M. C. Mol, T. Muselle, I. De Graeve, G. Van Assche, G. Scheltjens, B. Van Mele, H. Terryn, *Electrochem. Commun.* **2011**, *13*, 169.
[22] A. Davoodi, J. Pan, C. Leygraf, R. Parvizi, *Int. J. Hydrogen Energy* **2011**, *36*, 2855.
[23] N. C. W. Kuijpers, W. H. Kool, P. T. G. Koenis, K. E. Nilsen, I. Todd, S. van der Zwaag, *Mater. Charact. 49*, **2002**, 409.